THE JOURNAL OF PHYSICAL CHEMISTRY B

ARTICLE

pubs.acs.org/JPCB

Atomic Scale Determination of Enzyme Flexibility and Active Site Stability through Static Modes: Case of Dihydrofolate Reductase

Marie Brut,[*,†,‡,§] Alain Estève,[†,‡] Georges Landa,[†,‡] Guillaume Renvez,[†,‡] Mehdi Djafari Rouhani,[†,‡] and Marc Vaisset[†,‡]

[†]LAAS-CNRS, Université de Toulouse, 7 avenue du Colonel Roche, F-31077 Toulouse, France

[‡]Université de Toulouse, UPS, INSA, INP, ISAE, LAAS, F-31077 Toulouse, France

[§]Department of Structural Biology, Stanford University School of Medicine, Stanford, California, United States

ABSTRACT: A Static Mode approach is used to screen the biomechanical properties of DHFR. In this approach, a specific external stimulus may be designed at the atomic scale granularity to arrive at a proper molecular mechanism. In this frame, we address the issues related to the overall molecular flexibility versus loop motions and versus enzymatic activity. We show that backbone motions are particularly important to ensure DHFR domain communication and notably highlight the role of *a* α-helix in Met20 loop motion. We also investigate the active site flexibility in different bound states. Whereas in the occluded conformation the Met20 loop is highly flexible, in the closed conformation backbone motions are no longer significant, the Met20 loop is rigidified by new intra- and intermolecular weak bonds, which stabilizes the complex and promotes the hydride transfer. Finally, while various simulations, including I14 V and I14A mutations, confirm that Ile14 is a key residue in catalytic activity, we isolate and characterize at the atomic scale how a specific intraresidue chemical group makes it possible to assist ligand positioning, to direct the nicotinamide ring toward the folate ring.

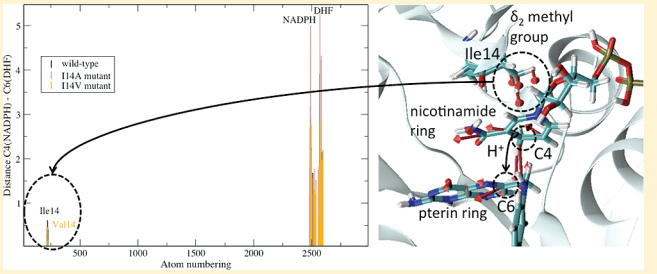

1. INTRODUCTION

Dihydrofolate reductase (DHFR) is found in most of living organisms, exhibiting an important structural homology despite a low sequence homology. In the presence of NADPH cofactor, DHFR catalyzes the reduction of 7,8-dihydrofolate (DHF) to 5,6,7,8-tetrahydrofolate (THF). Its role is essential for the synthesis of purine nucleotides and thymidilate, and consequently, for cell division. Inhibiting DHFR results in the perturbation of DNA synthesis leading to cell death. For this reason, this enzyme has been extensively studied for therapeutic purpose[1] and is currently a target, notably for chemotherapies, malaria, or tuberculosis treatments. It is still widely investigated as a model system to explore the relationship between conformational changes and catalytic activity.[2,3] The structure of DHFR was first solved more than 30 years ago;[4,5] it consists of the adenosine binding subdomain connected to a major subdomain via the enzyme active site.[6] The major domain, also called the loop subdomain, contains three flexible loops that are shown to play a crucial role in ligand binding,[7,8] catalysis, and product release: the Met20 loop (residues 9−24), the F-G loop (residues 116−132), and the G-H loop (residues 142−150) (see Figure 1.a).

The catalytic cycle of DHFR includes the following successive steps: NADPH cofactor binding, dihydrofolate binding, hydride transfer from NADPH to dihydrofolate and protonation, and release of tetrahydrofolate and cofactor. During this cycle, in solution, two conformations of the central portion of the Met20 loop (16−19 residues) have been observed: closed and occluded, depending on the ligand-bound state[8,9] (see Figure 1b). When only the folate substrate (FOL) is bound, the Met20 loop is found in an occluded conformation. This state is stabilized by the formation of hydrogen bonds between Asn23 in the Met20 loop and Ser148 in the G-H loop. When the nicotinamide cofactor is also bound, DHFR is found in a closed conformation: hydrogen bonds between Asn23 and Ser148 are disrupted, while new hydrogen bonds are formed between Gly15/Glu17 in the Met 20 loop and Asp122 in the F-G loop. The Met20 loop then covers up the cofactor, while the nicotinamide ring, in particular, is stabilizing the complex and protecting it from solvent.

In this work, we use a recently introduced method, the Static Modes method,[10−12] which makes it possible to efficiently screen the deformation response of a molecule submitted to an external excitation in a systematic manner. This method allows us to revisit some of the main enzyme biomechanical characteristics with an unpreceding atomic-scale degree of precision. Along this line, we investigate the Met20 loop motion between the closed and occluded conformations, in relation to the ligand-bound state of the enzyme. We evaluate and characterize the propensity of the Met20 loop to undergo conformational changes in the presence and absence of the nicotinamide ring. We also unravel

Received: October 14, 2010
Revised: December 14, 2010
Published: February 2, 2011

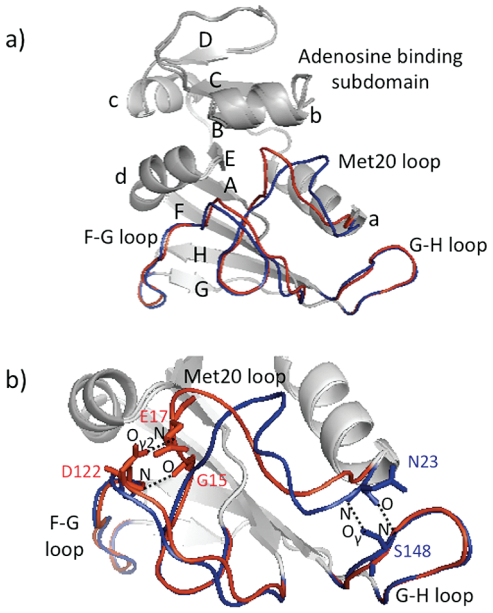

Figure 1. Overlay of two conformations of dihydrofolate reductase: with the Met20 loop in closed state (in red) and occluded state (in blue). Both conformations correspond, respectively, to 1RX2 and 1RX7 PDB files. Part (a) is an overall view of the enzyme. α-helices are labeled from a to d, and β-sheets from A to H. Part (b) is a close-up view of the loop domain, with annotated interactions between Met20 loop and F-G and G-H loops.

the detailed atomic-scale mechanism that establishes a crucial relation between the active site structure and the stability of the folate/cofactor complex, ensuring the catalysis activity.

2. METHODS

2.1. Structures. Two conformations of *E. coli* dihydrofolate reductase are used in this work, in reference to previous theoretical studies[6,7,13] that investigate the changes in flexibility of the enzyme upon cofactor binding. The case reported here depicts the conformational changes occurring during the transition from the binary complex E:FOL to the ternary complex E:FOL:NADPH. Another possibility was the study of the transition E:NADPH to E:NADPH:FOL, i.e., the substrate binding, which occurs at the beginning of the catalytic cycle. In this work, we have chosen to deal with the former case to position our approach in comparison to traditional methods such as molecular dynamics, and to highlight the new possibilities it offers.

The crystal structures of 1RX7 and 1RX2 are extracted from the Protein Data Bank. They correspond respectively to the occluded conformation (substrate-bound DHFR), and the closed conformation (cofactor and substrate-bound DHFR). Both structures are treated with the same procedure. They are first subjected to a total energy minimization. The AMBER 9 package[14] with the ff99SB[15] force field and an implicit solvent model are used to generate the conformations at the equilibrium and to extract their Hessian matrix. The matrix elements, which represent the force parameters describing atomic interactions, are then treated to compute the Static Modes.

2.2. Static Mode Calculation. A Static Mode is the molecular deformation related to a perturbation exerted on a specific atom in a specific direction. The Hessian matrix elements are used to simulate the excitations of the atoms in a systematic manner.[10]

The translation and rotation coordinates are first discarded, so that one ends up with a $(3N - 6) \times (3N - 6)$ matrix, with N being the number of atoms in the molecule. A constraint, in the sense of Lagrange, is then imposed on the molecule. Using the harmonic approximation, the force vector can be expressed as the gradient of the energy, written in terms of the Hessian matrix:

$$F_i = \sum_j H_{ij} x_j \qquad (1)$$

.H_{ij} represents the Hessian matrix elements and x_j the Cartesian coordinates of the atomic displacements from the equilibrium configuration. In the next step, we assume a given displacement x_l, resulting from the application of a force F_l. Under these conditions, x_l is the Lagrange constraint while F_l acts as a reaction force. In the algorithm, the l^{th} line of H, i.e., the equation containing F_l (the constraint equation) is eliminated from the set of eqs 1. Denoting by B the l^{th} column of the H (i.e., the terms containing x_l), and by A the remaining $(3N - 7) \times (3N - 7)$ matrix, we now solve the set $AX + B = 0$. The solution X is a Static Mode; it represents the atomic displacements imposed by the constraint. More details about the Static Mode methodology can be found in ref 10. The process is iterated for each atom and results in the mapping of all of the possible deformations of the molecule. The corresponding modes are stored in a data bank for post-treatment, simplifying the procedure and saving computer time. For the DHFR (2489 atoms), the calculation of the whole Static Mode requires 80 min of CPU time (2.8 GHz Intel dual core processor).

2.3. Discussion. Comparing our Static Modes approach to full MD, two questions may arise. The first concerns the robustness of the approach: Are similar effects observed starting with various close configurations? The atomic displacements in different Static Modes being determined via the inversion of the Hessian matrix, they are mainly governed by the largest element of this matrix, i.e., largest force constants, corresponding to the most rigid parts of the molecule and being at the origin of the high frequency Normal Modes. As long as these higher force constants are not seriously modified, the approach can be considered as robust. It is expected that the most rigid parts of the molecules are not subject to large changes in configurations close to that observed experimentally. The same approximation is frequently used in simpler MD simulations, where these parts are considered to be completely rigid. This assumption has also been verified in all cases investigated, including that reported in this work, where agreement with experimental data, reported in the literature, is observed at the first trial.

The second question then arises. What is the propagation time of the atomic displacement from the excited atom toward the observed region? Here also, the displacements are transmitted through the most rigid parts of the molecules and dampened when traveling along the softest regions. The propagation time is again governed by the high frequency part of the Normal Modes, in contrast to large natural deformations of the molecules governed by the low frequency part of the spectra. In this sense, the static nature of the modes used in our approach can be justified.

Beyond these general considerations, as developed in this work, the main goal of the Static Mode approach is to sufficiently simplify the dynamics to allow for the investigation of the effects of a huge number of external excitations with a reasonable computing effort.

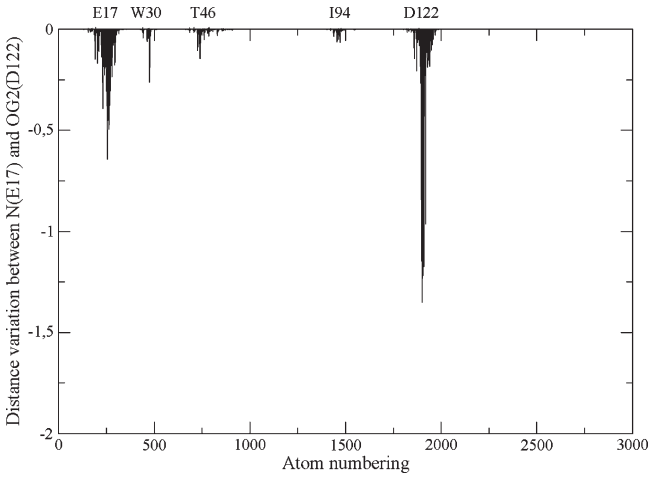

Figure 2. Distance variations between the NH(E17) and CγO2(D122) groups induced by the optimized excitation of each atom of the occluded DHFR (in Angstrom). Forces are all normalized to 1 eV/A.

2.4. Force Optimization. Once calculated, the modes can be used in a post-treatment procedure to explore a particular physicochemical mechanism of the protein in its intimate relation with a specific external excitation, single or multiple, as defined by the operator. In the present work, the post-treatment has as its main objective the identification of the atoms implied in the loop motion and the complex stability. In view to explore the structural changes, we optimize the constraints to adjust some given interatomic distances in the complexes. This problem is a constrained optimization problem: while conserving the amplitude of the force applied on the atom N_0, we optimize its direction to get the maximum distance variation between two atoms N_1 and N_2. We extract two matrices (3×3), $\mathbf{m}_{N1}$ and $\mathbf{m}_{N2}$ from the Static Modes, containing N_1 and N_2 displacements, resulting from the application of three forces in the x, y, z directions, on the atom N_0. The N_1N_2 distance variation is associated to the matrix $\mathbf{m} = \mathbf{m}_{N1} - \mathbf{m}_{N2}$. The optimized direction is given by the largest eigenvalue of $\mathbf{m}^t\mathbf{m}$ matrix and is determined by the iterative power method.

3. RESULTS

3.1. Loop Motion. Previous studies, using B-factors, have suggested that loop flexibility depends on the ligand-bound state of the enzyme.[16,17] In the closed state, in the presence of both ligands, low B-factor values are found, suggesting little motions of the loops. In the case of the occluded state, when only the folate is bound, higher B-factor values are found, showing larger motion of the loop.

We have successively optimized the excitation of all of the atoms of the molecule in the closed and occluded conformations to maximize the variation of the following distances: the distance between CO(G15) and NH(D122), between NH(E17) and COγ2(D122), between CO(N23) and NH(S148), and between NH(N23) and COγ(S148). By doing this, we can evaluate how the protein conformation drifts from the closed to the occluded conformation, by breaking hydrogen bonds between E17 (or G15) and D122 or by creating a new bond between N23 and S148. Along the same lines, we can characterize the conformational drift from the occluded to the closed conformation by breaking the N23−S148 hydrogen bond or by creating new bonds between E17−D122 and G15−D122.[7]

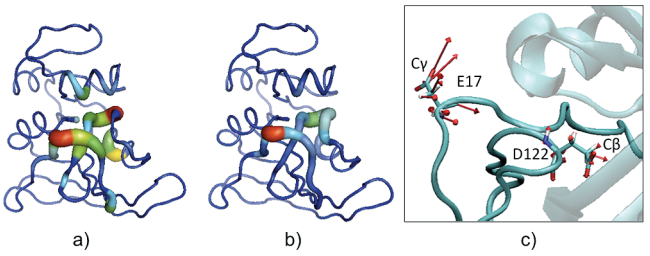

Figure 3. Representation of the residues involved in the distance variation between the NH(E17) and CγO2 (D122) groups (see Figure 1) on the occluded molecule (blue to red for minimal to maximal amplitudes). On the left (a), colors are assigned to residues according to Cα atom displacements. In the middle (b), colors are assigned in relation to the average atomic displacement per residue. On the right (c), a zoom of the forces applied on E17 and D122 are represented. The norm is proportional to the distance variation.

3.1.1. E17−D122 Distance. When the folate only is bound, Met20 is in the occluded conformation. We start from this structure to show how to close the loop. The aim is to depict the main intra molecular actors allowing us to switch from the occluded to the closed state. We therefore apply a force on each atom of the molecule with the objective of selecting the force vector orientation that corresponds to the maximum variation of E17−D122 distance. Figure 2 shows the distance variations for each optimized constraint applied on each atom of the molecule. We clearly see two main peaks, reaching −0.65 and −1.35 Å, corresponding, respectively, to E17 and D122 atoms, but interestingly, also many smaller variations, corresponding to other residues including W30, T46, and I94. For an easier readability of the graph, we have reported these variations on the molecule with colors from blue to red for minimal to maximal amplitudes (see Figure 3). Three figures are provided: the first one (a) represents the distance variations due to Cα excitation (i.e., variations correlated with backbone motions); on the second one (b), the colors correspond to the average of distance variations per residue, allowing us to estimate the side chains contribution.

In Figure 3a, one can see that, concerning the backbone role, E17 and D122 Cα atoms induce the maximal bond closure. Other Cα atoms of Met20 and FG loops, respectively of R12−N18 and D116−P126 residues, are also implied in the closure. Further, Cα atoms of the following residues: W30−F31 (a α-helix), H45−T46 and S49−I50 (b α-helix), and I94 (E β-sheet), are also involved in Met20 loop motion.

These results are particularly interesting because all of these residues have been identified for their role in the closed/occluded transition.[18] Notably, contacts between the Met20 loop and the b α-helix are important in the allosteric transition. Their motions are highly correlated and supposed to play a role in the mechanism of domain communication. Furthermore, these residues are strongly conserved in the sequence-known DHFR.[19] It implies that they are crucially involved in the enzymatic mechanism, and moreover, that they can be envisaged as possible targets.

From Figure 3b, we can deduce that, considering the entire residue contribution, only G15−M20 (Met20 loop) and E120−F125 (F-G loop) atoms can really contribute to Met20 motion. The deformation easily propagates through backbone atoms, while only side chains of the closest residues are really implied in Met20 motion. This result is not surprising since, in the occluded conformation, many weak bonds

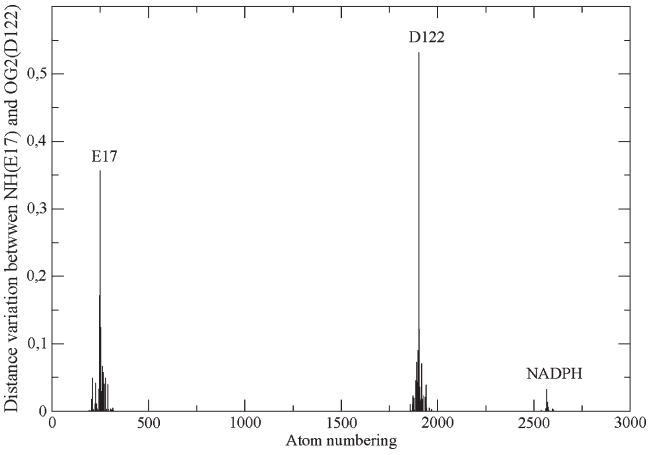

Figure 4. Distance variations between NH(E17) and CγO2 (D122) group induced by the optimized excitation of each atom of the closed DHFR (in Angstrom). Forces are all normalized to 1 eV/A.

between side chain residues are disrupted and cannot propagate the deformation.

While the literature exclusively addresses the overall mechanistic molecular properties at the residue granularity, Static Modes make it possible to explore these issues at the atomistic resolution; hence, it becomes possible to design an excitation (a force vector on a specific atom or multiple force vectors on a collection of atoms) and to depict its associated molecular deformation response. In Figure 3c, we have represented the optimized forces computed to get the deformation previously described. Their direction is an accurate indication of how constraining the DFHR atoms are toward getting the desired loop motion, while their norm is proportional to the deformation amplitude that we obtained. In other words, the longer the arrow is, the easier it is to minimize the E17−D122 distance. Much information can be extracted from this representation, notably an easy reading of the atom contribution. For instance, it is remarkable to notice that the optimum way to move NH(E17) and COγ2(D122) is not to constraint these atoms themselves, but Cγ and Cβ atoms from E17 and D122 residues, respectively.

When the nicotinamide cofactor is also bound (closed conformation), an equivalent exploration of the Static Modes to maximize E17−D122 (as presented in Figure 4), indicates that the E17 and D122 peaks are still visible, but with a smaller amplitude (0.35 and 0.53 Å, respectively). In addition, all other protein residues expected from the previous case have disappeared (compared with Figure 2). This means that the molecule is much more rigid in the closed conformation than when the nicotinamide cofactor is unbound. The set of weak bonds, formed with residues in the F-G loop and with the ligands in the binding pocket, stabilizes the Met20 loop-closed conformation. It makes it very difficult to stretch the E17/D122 bond. Such a conclusion corroborates a single-molecule force spectroscopy work,[20] showing that ligand binding increases DHFR mechanical stability, because of the network of protein−ligand interactions. Furthermore, a small peak (0.3 Å) corresponding to NADPH atoms is visible. Again, thanks to the atomic resolution available, one can observe that the concerned NADPH atoms belong to the sugar ring linked to the nicotinamide, which appears to be really close in space to E17 and D122 residues. This finding confirms and details the cofactor binding implication in Met20 loop stabilization in a closed state.

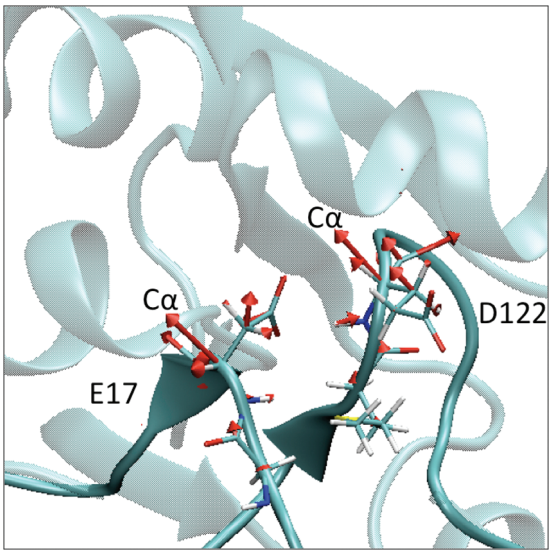

Figure 5. Representation of the forces applied on the closed DHFR atoms to obtain an optimized closure of NH(E17) and CγO2 (D122). The norm represented is proportional to the distance variation.

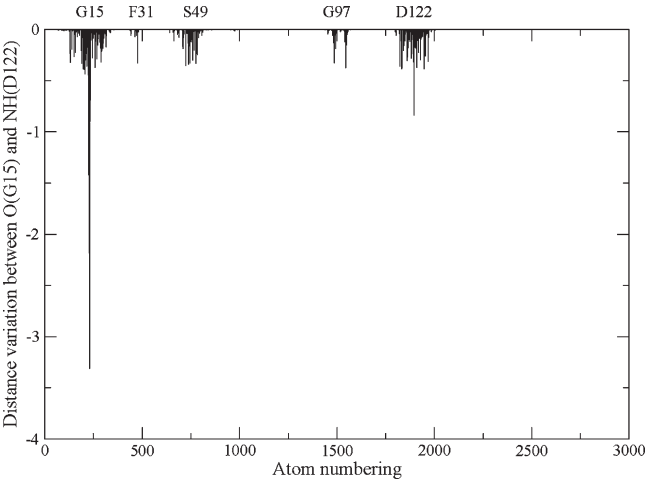

Figure 6. Distance variations between CO(G15) and NH(D122) group induced by the optimized excitation of each atom of the occluded DHFR (in Angstrom). Forces are all normalized to 1 eV/A.

Finally, as shown in Figure 5, contrary to what we have found for the occluded state, the optimum way to move NH(E17) and COγ2(D122) atoms is now to constrain the α-carbon atoms, the side chains are stabilized by new interactions. It confirms that DHFR mechanical properties are changed in a closed state, distant motions are hindered (Figure 5 is to be compared to Figure 3c).

3.1.2. G15−D122 Distance. Along the same line, we now focus on the G15−D122 distance that also characterizes the occluded DHFR conformation. Figure 6 shows CO(G15)−NH(D122) distance variations obtained for the occluded state of DHFR. Again, it is not surprising to notice that both major peaks, reaching −3.30 and −0.85 Å, respectively, correspond to G15 and D122 atoms, respectively. Other significant variations are induced by excitations applied on the following residues: V13−M16 and M20 (Met20), S49 (*b* α-helix), D116−A117 and G121−T123 (F-G loop). All of these residues are also

dx.doi.org/10.1021/jp109874z |*J. Phys. Chem. B* 2011, 115, 1616–1622

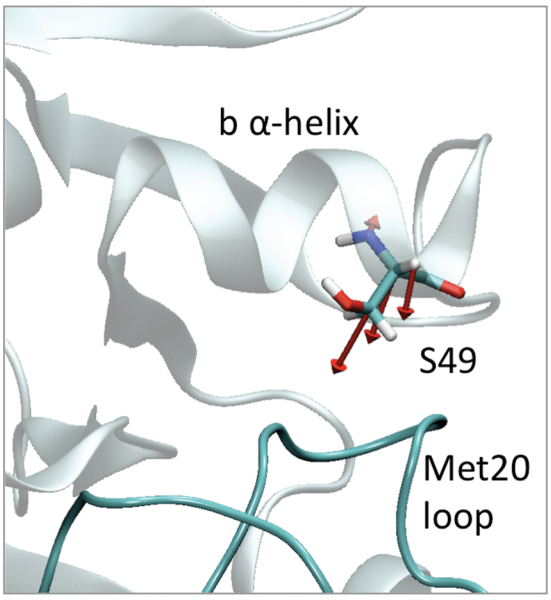

Figure 7. Representation of the forces applied on the occluded DHFR atoms to obtain an optimized closure of CO(G15) and NH(D122). The norm represented is proportional to the distance variation.

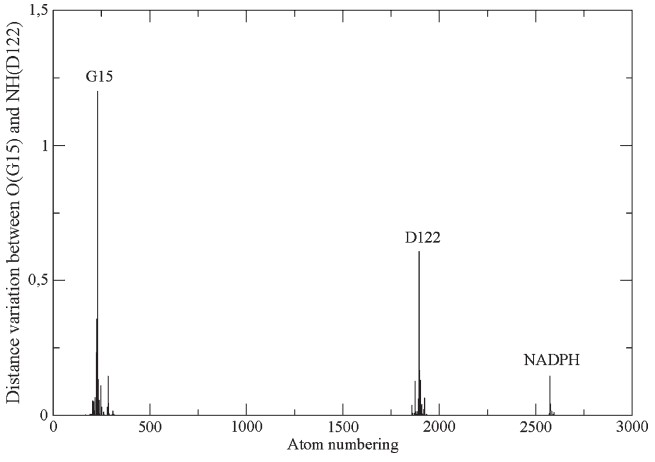

Figure 8. Distance variations between CO(G15) and NH(D122) group induced by the optimized excitation of each atom of the closed DHFR (in Angstrom). Forces are all normalized to 1 eV/A.

involved in E17−D122 (see Figure 2). It is not surprising since E17−D122 and G15−D122 are interconnected and localized in space. Finally, the hydrogen bonds existing between N18 and S49[21] allow us to understand how S49 is involved here.

Now, if we consider the average contribution per residue, only G15 and M16 residues are conserved. As seen previously, we can conclude that backbone motions are responsible for the communication between domains. This information is also clearly visible from the atomistic picture given in Figure 7, with the force vector representation. The forces that drive S49 (*b* α-helix) are especially highlighted in the figure.

We have performed the same calculations for the DHFR in the closed state. The results are presented in Figure 8. Both G15 and D122 peaks are conserved with smaller amplitudes (1.47 and 0.68 Å, respectively) illustrating the overall increase in molecular rigidity. All other contributions are no longer represented. However, as in the previous case, a new peak appears, indicating the contribution of two carbon atoms of the sugar ring linked to the nicotinamide ring. Similar to our conclusions concerning the E17−D122 distance calculations, the nicotinamide cofactor stabilizes the overall conformation. It makes it difficult to drive a loop motion via the external stimuli considered in this work.

3.1.3. N23−S148 Distance. The variations of the N23−S148 distance, characteristic of the occluded state, are now considered. Results are not shown due to their similarities with the characteristics found above: the residues that induce a maximal distance variation are N23 and S148, themselves, as well as the closest Met20 loop and G-H loop residues (A19-L24 and N147−S150, respectively). Again, some residues of *a* α-helix (A29-F31) and F-G loop (H114−I115) are also active. This result was expected since the G-H does not undergo significant change. By measuring N23−148, we evaluate how the Met20 loop moves toward the G-H loop and back. It is thus consistent to identify some F-G loop residues, which push the Met20 loop toward the G-H loop, and *a* α-helix residues, correlated with Met20.

In this first part of the work, we decided not to go too far into the atomistic details accessible by our methodology. Our method allows the analysis of the displacements and their associated excitations at the atomic scale. Beyond this, our aim is to show how to use the Static Modes to find intrinsic properties of flexibility and motion directly comparable with experimental results where the scale is more at the level of an entire residue. In this preliminary work, we have identified which parts of the molecule (residues, Cα atoms, side chains) are inferred to cause Met20 loop motions. Results are consistent with contacts between residues, domain communication, and networks of residues, an ensemble of results previously identified in the literature and here provided by a single Static Mode calculation run. This study has also shown a difference of flexibility depending on the ligand-bound state. In the closed conformation, i.e., in the ternary complex, because of new bonds formed inside the enzyme and between the enzyme and the ligands, deformations are much more difficult to produce via external excitations. The overall structure is more rigid, helping to stabilize the folate in a geometry favorable to the catalysis reaction. In the next section, we go further into the atomistic biomechanical details of the enzyme catalytic function.

3.2. Active Site. Using the same Static Mode approach, we now focus on the active site, specifically on the enzyme catalytic mechanism versus systematic molecular excitations.

3.2.1. Distance between C4(NADPH) and C6(DHF). DHFR catalytic function consists in the hydride transfer from a donor atom of the nicotinamide ring (C4), to an acceptor atom of the folate pterin ring (C6). The vicinity of both ligands in the complex enhances this mechanism. The perturbation of the ligand positions results in a loss of enzymatic activity. We used the same optimization protocol to evaluate the role of active site flexibility on ligand positioning. Figure 9 shows the distance variation between C4 and C6 atoms. A logarithmic representation is used to facilitate the readability. The values are very small, consistent with previous conclusions about the high active site stability in the closed conformation. The major peaks, reaching 0.04 and 0.08 Å, respectively, correspond to the cofactor and substrate atoms, mainly to the ring atoms, as seen in Figure 10. However, it is remarkable to notice another peak on the left, corresponding to Ile14 atoms, more exactly to Ile14 δ2 methyl group. While the role of this residue has already been highlighted in previous studies,[6,19,21−23] its exact atomic-scale mechanism is

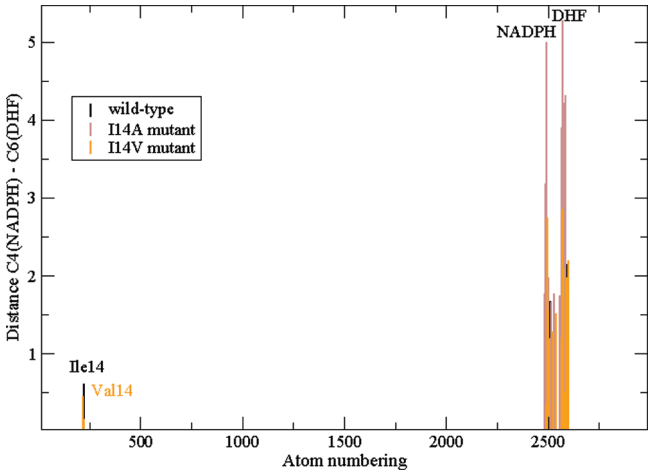

Figure 9. Logarithmic representation of the distance variations between C4(NADPH) and N6(DHF) atoms induced by the optimized excitation of each atom of the closed DHFR. Three cases are treated: the nonmutant DHFR (in black), I14 V (in orange), and I14A (in gray).

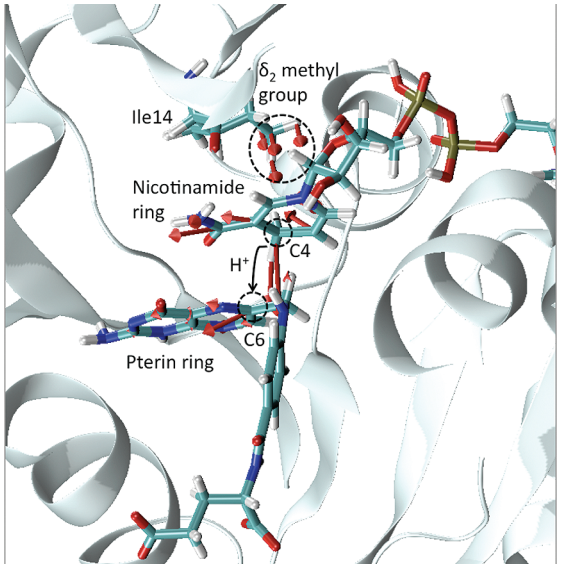

Figure 10. Structure of the catalytic site. The nicotinamide ring (NADPH) and the pterin ring (DHF) are shown, as well as C4 and C6 atoms involved in the hydride transfer. The optimized forces applied on Ile14 to maximize the distance variation between C4(NADPH) and N6(DHF) are represented.

here detailed, to the best of our knowledge, for the first time. Its side chain atoms pack against the nicotinamide ring of the cofactor (C4 region), pushing it toward the folate pterin ring (C6 atoms and neighbors), as illustrated in Figure 10. The driving forces follow the direction of Ile14 methyl group−C4(NADHP)−C6(DHF) alignment, perpendicularly to the pterin and nicotinamide ring plan.

To enlighten the role played by the Ile14 methyl group, this residue was successively replaced with valine (I14 V) and alanine (I14A). The substitutions were designed using 1RX2 PDB file and Pymol molecular graphics system.[24] I14A mutation is less bulky since its short side chain is a simple methyl group. As a consequence, it should alter the weak bonds formed with the nicotinamide ring. Again, we used the same procedure as above with the new structure containing the I14A mutant: a preliminary total energy minimization was run, followed by the Static Mode calculation and force optimization. The optimization result is presented in Figure 9 (in gray). In comparison to the nonmutant results, both peaks corresponding to the nicotinamide and pterin ring atoms still appear. However, the amplitudes are much more important, reaching 2 Å. Furthermore, there is no distance variation corresponding to the constraint applied on I14A. Ala14 is too short to pack against the nicotinamide ring. The active site becomes significantly more flexible, which suggests a probable loss of activity concerning the hydride transfer. This result corroborates the important role played by the Ile14 side chain in the complex stabilization and is consistent with a recent experimental study from Stojkovic et al.[25] This work suggests that I14A mutation modulates the hydride transfer, and more generally, that decreasing the constraint imposed on the cofactor, through a shorter side chain, perturbs the catalytic activity.

In order to go further in our proposition, the same work was done using the I14 V mutant. Since valine is shorter than isoleucine (the $\delta 2$ methyl group is missing), this work allows us to complete our conclusion. The results are shown in Figure 9 (in orange). Two peaks, with amplitudes around 0.17 and 0.2 Å, correspond to NADPH and DHF atoms, respectively. These values are much lower than those found with I14A mutants, but approximatively three times larger than those of the wild-type enzyme. This leads to the conclusion that the side-chain length is essential for the complex stabilization. A third peak is visible, corresponding to the CO group of Val14, which is oriented toward the NADPH cofactor. This group establishes a hydrogen bond with the carboxamide N of NADPH and contributes to modulate the nicotinamide ring position. Yet, the amplitudes indicate that the effect is less than that for Ile14. The comparison of the wild-type enzyme, I14A and I14 V allows us to characterize the role of Ile14 side chain in the nicotinamide ring displacement. Its length is essential to create a spatial constraint that optimizes the active site configuration. Moreover, it plays a key role in complex stabilization, necessary to promote the hydride transfer from donor to acceptor. It is worth noting that this residue is highly conserved in DHFR.[22,23]

4. CONCLUSIONS

The Static Mode method is applied to address basic mechanical mechanisms of *E. coli* DHFR with an atomic resolution: the loop motion necessary to maintain catalytic activity and the role of some active site residues. Our results indicate that backbone motions are particularly important to provide DHFR domain communication. We notably highlight the role of *a* α-helix in Met20 loop motion. This work also allows us to compare the active site flexibility in different ligand-bound states. In the occluded conformation, in which the Met20 loop is highly flexible, the backbone motions promote its conformational changes. However, when the active site adopts a closed conformation, the backbone motions are no longer significant and the Met20 loop is rigidified by new intra- and intermolecular weak bonds, which stabilize the complex and promote the hydride transfer. No distant residue appears to be involved in the active site stability, which disagrees with the mechanism of a network of promoting motions, supported by the QM/MM studies of Hammes-Shiffer et al.[22] or the kinetic studies of Sikorski et al.[26] On the contrary, a network of weak bonds rigidifies the structure in a configuration favorable to the hydride

transfer. Only a few residues, closed to the active site, can promote the hydrogen tunneling. Their short-range and localized motion helps in modulating the C4(NADPH)−C6(DHF) distance, and consequently, the activation barrier. This result supports the hypothesis of "localized promoting motions", already suggested in previous experimental and theoretical studies.[27−29]

In particular, we show that Ile14 is a key residue in the stabilization of the active site. Its exact atomistic behavior is detailed. We find that the stabilization is operated by Ile14 $\delta 2$ methyl termination, which is aligned with C4(NADPH) and C6(FOL) atoms, determining their respective positions to favor the hydride transfer. Calculations using I14A and I14 V mutants confirmed that the Ile14 side chain assists in ligand positioning, directing the nicotinamide ring (donor) toward the folate ring (acceptor). It is remarkable that most of the residues we have identified to play an essential role in enzyme activity are strongly conserved residues.

It is accepted today that flexibility is an enzyme characteristic necessary to its activity. However, there is currently a lack of the structural or biochemical information required to understand in detail how flexibility is correlated with functional activity. Thanks to the amount of structural and dynamic data collected on DHFR, this molecule represents an excellent model system for applying our method, comparing our results with known characteristics of the enzyme, and evaluating its contribution. Here, within a single calculation, we have identified residues involved in loop motion and catalytic activity that have been collected over years and with many different techniques in the literature. We show that our method authorizes an atomic scale expertise of this information. We also demonstrate its usefulness in the efficient treatment of mutations. It allows us to think that the Static Mode method can be used for the exploration of molecular mechanisms, and as confirmed by I14Aand I14 V mutation examples, for de novo design strategies.

AUTHOR INFORMATION

Corresponding Author

*Tel: +1 (650) 725 0754; Fax: +1 650 723 8464; E-mail: mbrut@stanford.edu.

ACKNOWLEDGMENT

We thank the CALMIP Supercomputer Center for CPU resources. We also thank projects ANR-NANOBIOMOD and ITAV-ALMA for financial support.

REFERENCES

(1) Schweitzer, B. I.; Dicker, A. P.; Bertino, J. R. *FASEB J.* **1990**, *4*, 2441–2452.

(2) Radkiewicz, J. L.; Brooks, C. L. *J. Am. Chem. Soc.* **2000**, *122*, 225–231.

(3) Boehr, D. D.; McElheny, D.; Dyson, H. J.; Wright, P. E. *Science* **2006**, *313*, 1638–1641.

(4) Matthews, D. A.; Alden, R. A.; Bolin, J. T.; Freer, S. T.; Hamlin, R.; Xuong, N.; Kraut, J.; Poe, M.; Williams, M.; Hoogsteen, K. *Science* **1997**, *197*, 452–455.

(5) Bolin, J. T.; Filman, D. J.; Matthews, D. A.; Hamlin, R. C.; Kraut, J. *J. Biol. Chem.* **1982**, *257*, 13650–13652.

(6) Schnell, J. R.; Dyson, H. J.; Wright, P. E. *Annu. Rev. Biophys. Biomol. Struct.* **2004**, *33*, 119–140.

(7) Osborne, M. J.; Schnell, J.; Benkovic, S. J.; Dyson, H. J.; Wright, P. E. *Biochemistry* **2001**, *40*, 9846–9859.

(8) McElheny, D.; Schnell, J. R.; Lansing, J. C.; Dyson, H. J.; Wright, P. E. *Proc. Natl. Acad. Sci. U.S.A.* **2005**, *102*, 5032–5037.

(9) Sawaya, M. R.; Kraut, J. *Biochemistry* **1997**, *36*, 586–603.

(10) Brut, M.; Estève, A.; Landa, G.; Renvez, G.; Djafari Rouhani, M. *Eur. Phys. J. E* **2009**, *28*, 17–25.

(11) Brut, M.; Estève, A.; Landa, G.; Renvez, G.; Djafari Rouhani, M.; Vaisset, M.; Gauchard, D. *Mater. Sci. Eng., B* **2010**, *169*, 23–27.

(12) Brut, M.; Estève, A.; Landa, G.; Dkhissi, A.; Renvez, G.; Djafari Rouhani, M.; Gauchard, D. *Tetrahedron* **2010**, *66*, 9123–9128.

(13) Rod, T. H.; Radkiewicz, J. L.; Brooks, C. L., III *Proc. Natl. Acad. Sci. U.S.A.* **2010**, *100*, 6980.

(14) Case, D. A.; Darden, T. A.; Cheatham, III, T. E.; Simmerling, C. L.; Wang, J.; Duke, R. E.; Luo, R.; Merz, K. M.; Pearlman, D. A.; Crowley, M.; Walker, R. C.; Zhang, W.; Wang, B.; Hayik, S.; Roitberg, A.; Seabra, G.; Wong, K. F.; Paesani, F.; Wu, X.; Brozell, S.; Tsui, V.; Gohlke, H.; Yang, L.; Tan, C.; Mongan, J.; Hornak, V.; Cui, G.; Beroza, P.; Mathews, D. H.; Schafmeister, C.; Ross, W. S.; Kollman, P. A. *AMBER 9* ;University of California: San Francisco, 2006.

(15) Hornak, V.; Abel, R.; Okur, A.; Strockbine, B.; Roitberg, A.; Simmerling, C. *Proteins* **2006**, *65*, 712–725.

(16) Bystroff, C.; Oatley, S. J.; Kraut, J. *Biochemistry* **1990**, *29*, 3263–3277.

(17) Bystroff, C.; Kraut, J. *Biochemistry* **1991**, *30*, 2227–2239.

(18) Chen, J.; Dima, R. I.; Thirumalai, D. *J. Mol. Biol.* **2007**, *374*, 250–266.

(19) Ainavarapu, S. R. K.; Li, L.; Badilla, C. L.; Fernandez, J. M. *Biophys. J.* **2005**, *89*, 3337–3344.

(20) Bernacki, K.; Kalyanaraman, C.; Jacobson, M. P. *J. Biomol. Screen* **2005**, *10*, 675–681.

(21) Adams, J. A.; Fierke, C. A.; Benkovic, S. J. *Biochemistry* **1991**, *30*, 11046–11054.

(22) Watney, J. B.; Agarwal, P. K.; Hammes-Schiffer, S. *J. Am. Chem. Soc.* **2003**, *125*, 3745–3750.

(23) Agarwal, P. K.; Billeter, S. R.; Rajagopalan, P. T. R.; Benkovic, S. J.; Hammes-Schiffer, S. *Proc. Natl. Acad. Sci. U.S.A.* **2002**, *99*, 2794–2799.

(24) The PyMOL Molecular Graphics System, Version 1.3, Schrödinger, LLC.

(25) Stojković, V.; Perissinotti, L. L.; Lee, J.; Benkovic, S. J.; Kohen, A. *Chem. Commun.* **2010**, *46*, 8974–8976.

(26) Sikorski, R. S.; Wang, L.; Markham, K. A.; Rajagopalan, P. T. R.; Benkovic, S. J.; Kohen, A. *J. Am. Chem. Soc.* **2004**, *126*, 4778–4779.

(27) Loveridge, E. J.; Tey, L.-H.; Allemann, R. K. *J. Am. Chem. Soc.* **2010**, *132*, 1137–1143.

(28) Swanwick, R. S.; Maglia, G.; Tey, L.-H.; Allemann, R. K. *Biochem. J.* **2006**, *394*, 259–265.

(29) Masgrau, L.; Roujeinikova, A.; Johannissen, L. O.; Hothi, P.; Basran, J.; Ranaghan, K. E.; Mulholland, A. J.; Sutcliffe, M. J.; Scrutton, N. S.; Leys, D. *Science* **2006**, *312*, 237–241.